

Buddy Compression: Enabling Larger Memory for Deep Learning and HPC Workloads on GPUs

Esha Choukse

University of Texas at Austin
esha.choukse@utexas.edu

Michael B. Sullivan
NVIDIA
misullivan@nvidia.com

Mike O'Connor
NVIDIA
moconnor@nvidia.com

Mattan Erez
University of Texas at Austin
mattan.erez@utexas.edu

Jeff Pool
NVIDIA
jpool@nvidia.com

David Nellans
NVIDIA
dnellans@nvidia.com

Stephen W. Keckler
NVIDIA
skeckler@nvidia.com

ABSTRACT

GPUs offer orders-of-magnitude higher memory bandwidth than traditional CPU-only systems. But, their memory capacity tends to be relatively small and can not be increased by the user. This work proposes Buddy Compression, a scheme to increase both the effective GPU memory capacity, and bandwidth, while avoiding the downsides of conventional memory-expansion techniques. Buddy Compression splits each compressed memory-entry between high-speed GPU memory and a slower-but-larger disaggregated memory pool or host-CPU memory, such that highly-compressible memory-entries are accessed completely from GPU memory, while incompressible entries source some of their data from off-GPU memory. We show that Buddy Compression achieves an average compression ratio of 1.9x for representative HPC applications and 1.5x for deep learning workloads, with a performance within 2% of an ideal system containing 100% high speed and high capacity memory. This makes Buddy Compression an ideal candidate for developers that require some additional memory capacity, and can tolerate minimal performance penalty.

1 INTRODUCTION

GPUs are widely used for many high-memory-footprint applications, including those for High Performance Computing (HPC) and Deep Learning (DL). HPC applications like weather prediction and the modeling of fluid and molecular dynamics have grown to require very large models [1, 2]. DL networks are also developing in a direction where either the model sizes are too big to run on GPUs, or they are large enough such that the only a small batch size can fit on the GPU, resulting in low utilization, and accuracy issues [3–5]. Today, applications with large memory footprints must: (i) scale out to many GPUs for capacity purposes (inefficient resource utilization) [6, 7], (ii) explicitly orchestrate data movement between the host CPU and the GPU to stay within device memory limitations (adding algorithmic complexity) [4, 8, 9], or (iii) rely on off-GPU memory accesses or Unified Memory [10] to automatically oversubscribe device memory (limiting performance) [11, 12]. In this paper, we explore memory compression as a solution to this challenge.

Main memory compression has been studied in detail for CPUs [13–17]. However, GPU-specific workloads and architectural



Fig. 1: In Buddy Compression, if a memory-entry (128B) does not compress sufficiently, part of it is accessed from the buddy-memory.

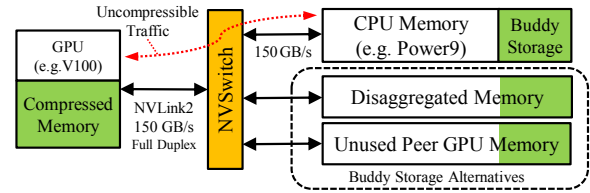


Fig. 2: A target system for Buddy Compression. Any larger NVLink-connected memory is used as buddy storage. Overall organization is like NVIDIA DGX-2 [20].

details pose very different trade-offs. For instance, the CPU solutions assume the compressed pages to be of different sizes and that they can be re-allocated as the compression ratios change [14–17]. Due to the immense device memory bandwidth, relying on such on-the-fly page re-allocations has a huge impact on throughput in GPUs [11].

While domain-specific compression [18, 19] has been explored to help with large workloads on GPUs, hardware memory compression to increase memory capacity for general purpose applications in GPUs remains unexplored.

In Buddy Compression, we compress the data and divide the compressed memory allocations between the GPU device memory and a larger-but-slower buddy-memory connected with a high-bandwidth interconnect (Figure 1). If a memory-entry is sufficiently compressed, it is sourced completely from device memory. If not, it is sourced from both device and buddy-memory. This design requires no re-allocations within the device memory as the data changes compressibility over time. A high-bandwidth interconnect like NVLink [20], OpenCAPI [21] or PCIe5.0 [22] is the enabling feature for this design, since it ensures low overhead accesses to the buddy-memory, as long as most of the data is in GPU device memory. Any remote memory that is connected to the GPU with a high-bandwidth interconnect is suitable for being used as buddy-memory (Figure 2). As we demonstrate in the rest of the paper, this design

maintains a good compression ratio and high performance, while avoiding the complexity and performance concerns of mapping CPU memory compression approaches on GPUs. To summarize the research contributions of this work:

- We provide an in-depth analysis of the data of representative GPU workloads and derive insights for effective GPU compression.
- We introduce the first design to use general-purpose compression to increase the memory capacity of GPUs. Buddy Compression is unique, since it does not require any additional data movement as the compressibility of the data changes.
- We show that Buddy Compression achieves 1.9x compression and performs within 2% of an ideal, high-memory-capacity GPU.
- Finally, we present a case study on DL training to understand the benefits and trade-offs of using Buddy Compression.

2 OVERVIEW

2.1 Target Workloads and Motivation

HPC Workloads. Several important HPC applications, ranging from fluid dynamics to weather prediction, have found GPUs to be the accelerator of choice. These models have outgrown GPU device memory [1, 2]. Today, scientists use either Unified Memory or multiple GPUs to scale the models. Device memory compression can be very useful for such cases. We use a subset of SpecAccel and DOE FastForward benchmarks to represent these HPC applications. The subset is chosen based on the confidence in the representativeness of the data values used in the benchmarks. All the discarded benchmarks seemed to have large portions of their working sets be zero, thereby having extremely high compression ratios.

DL Workloads. GPUs are currently the most popular choice for training deep neural networks. As these networks grow deeper and wider, they require more data and are inevitably hitting the memory-capacity wall, as we discuss in detail in Section 4.4. While many domain-specific solutions across the stack have been proposed to deal with this memory capacity challenge in deep learning training [6, 9, 19, 23–27], our proposal requires no algorithm-level changes, and applies to other classes of workloads as well. We use a set of convolutional neural networks (CNNs) and one recurrent neural network (RNN) to represent this class of workloads in our evaluation.

2.2 Related Work

There are two approaches to tackle memory limitations: compression, and domain-specific techniques. The graphics pipeline of most GPUs includes texture memory that is lossily compressed

offline using tailored compression algorithms [18, 28] in order to reduce the footprint of these textures. The deep learning space has domain-specific solutions across the stack [19, 24, 25]. Buddy Compression is orthogonal to most of these proposals. For instance, vDNN [25] proposes running large DL networks using manual offloading of data layer-by-layer. However, there are still cases where it fails, due to the inability to fit data required for just one layer [29]. Buddy compression can enable running larger networks with vDNN. To our knowledge, hardware compression is not currently used for general-purpose compute workloads on GPUs.

In CPUs, for decades, memory compression in various forms has been proposed and used as a solution to the memory capacity challenge. Most modern operating systems compress the swap space to reduce paging to disk [30]. There have been numerous proposals for hardware-accelerated main memory compression [13–17].

2.3 Relevant Modern GPU Technology

Unified Memory (UM). Unified Memory (UM), introduced in CUDA 8 for Pascal-class GPUs [10], allows sharing a single memory space across a heterogeneous node. Non-local UM requests either remotely access data through the GPU interconnect or result in transparent data migration with the placement of any piece of data being determined by a variety of heuristics [10, 31]. UM supports memory over-subscription, allowing UM-managed regions that are larger than the GPU device memory to be accessed without explicit data movement. This has not been widely adopted, since applications with large hot working sets experience frequent page faults and thrashing with Unified Memory, causing high performance overheads [29, 31, 32]. Similar solutions are available for AMD and ARM GPUs using Heterogeneous System Architecture (HSA) and CCIX [33, 34], and very recently, for Intel GPUs using Compute eXpress Link (CXL) [22].

High Bandwidth Interconnects. In recent years, high bandwidth interconnects like NVLink [35], openCAPI [21], and NVLink2 [20] have been used to alleviate the communication bottleneck in multi-GPU systems. Buddy Compression is made possible due to these high-bandwidth interconnects. NVLink2 provides 25GBps of full-duplex unidirectional bandwidth per brick. Modern compute-class V100 GPUs support six NVLink2 bricks per GPU, offering a bidirectional bandwidth of up to 150GBps (full-duplex), much higher than the 16GBps \times 16 PCIe3.0 full-duplex connection. The NVIDIA DGX-2 [20] workstation has sixteen V100 GPUs connected through an NVLink2 switch that supports the full 150GBps traffic between any two GPUs. IBM Power9 CPUs also support six NVLink2 bricks, allowing high-speed remote access to system memory [36].

Buddy Compression Target System. Given the trends in modern GPU nodes, the future-facing system we envision for Buddy Compression is shown in Figure 2. It is composed of NVSwitch-connected multi-GPU nodes with NVLink2-based access to a larger source of remote memory. In currently available systems, this remote memory could be the system memory of a Power9 CPU, or unused peer GPU memory. While we know of no current NVLink-connected disaggregated memory appliance, such a device is a natural extension of the technology that is being explored for servers [37,

Tab. 1: Details of the GPU Benchmarks Used

HPC SpecAccel		HPC FastForward	
351.palm	2.89GB	FF_HPGMG-FV	2.32GB
352.ep	2.75GB	FF_Lulesh	1.59GB
354.cg	1.23GB	DL Training	
355.seismic	2.83GB	BigLSTM	2.71GB
356.sp	2.83GB	AlexiNet	8.85GB
357.csp	1.44GB	Inception_V2	3.21GB
360.ilbdc	1.94GB	SqueezeNetv1.1	2.03GB
370.bt	1.21MB	VGG16	11.08GB
		ResNet50	4.50GB

38]. The high-bandwidth interconnect is what enables Buddy Compression. So, as long as the remote memory sources operate at the full NVLink2 bandwidth, Buddy Compression applies equally well. Any high bandwidth interconnect can be used in place of NVLink2.

2.4 Compression Design Considerations

There are some important design choices and challenges that need to be addressed in a compressed memory proposal. We present these design points in brief.

Compression Algorithms. A hardware memory compression algorithm should be fast and require little energy, yet result in high compression rates. *After comparing several algorithms [39–43], we choose Bit-Plane Compression (BPC) [43] for Buddy Compression.* BPC has been shown to have high compression ratios for GPU benchmarks when applied for DRAM bandwidth compression.

Compression Granularity. This is the unit of data that is compressed or decompressed together. A higher compression granularity requires less metadata, and generally results in higher compression. On the other hand, a lower compression granularity does not require as many read-modify-write operations. Most CPU main memory compression work uses a cache-block sized compression granularity to avoid these overheads. *We share this design decision, and, following the results of microbenchmarks [44], use a 128B memory-entry as the compression granularity for GPUs.*

Translation Metadata. The compressed size of each 128B memory-entry depends on its compressibility. This requires additional translation metadata to access compressed data. This metadata lookup generally lies on the critical path for every access to the memory. The layout of a compressed main-memory is somewhat similar in all previous work on main memory compression in CPUs. There is some space dedicated for the compression metadata, and the rest is arranged as variable-sized pages. Page size is decided by the compressibility of the data within a page.

Compressed Data Movement and Allocation. As data is written back to a compressed memory, value changes can lead to changes in compressibility. This means that a memory-entry can grow or shrink over time, leading to additional data movement [17]. Allocation granularity is closely related to the data movement overhead. For example, current systems allocate memory at page granularity. Changes in the size of one memory-entry can lead to data movement within and across the pages. However, if each memory-entry is separately allocated and translated, its size changes do not affect other data.

3 BUDDY COMPRESSION

3.1 Compressibility of Workloads

To estimate the possible gains from compression, it is imperative to first find how compressible the high-footprint GPU workloads are. To this end, we take memory dumps of the workloads running on a Tesla P100 GPU with an Intel Xeon E5 host. We intercept each GPU *malloc* and *free* API call (including variants for pinned and Unified Memory-managed memory) to dynamically track the current allocated regions in device memory. We divide the entire runtime of the workload into 10 regions, and at kernel boundaries of each region, take a memory dump of the allocated device memory.

Figure 3 shows the compression ratio of each benchmark using BPC compression [43] over its entire run. Note that these compression ratios are quite optimistic capacity compression, since they assume eight different compressed memory-entry sizes are available (0B, 8B, 16B, 32B, 64B, 80B, 96B, and 128B) and assume no page-packing overheads. That is, each memory-entry is individually compressed and allowed to occupy any of the above mentioned sizes. On average, the geometric mean of compression ratio for the HPC workloads is 2.51 for the HPC benchmarks and 1.85 for the DL benchmarks. This is a higher average as compared to prior work on CPU workloads [17], and can be attributed to the higher percentage of homogeneous data allocations (with a single uniform datatype). Prior work has established that Bit-Plane Compression works well for homogeneous data, and such homogeneity is prevalent in GPU workloads [43].

Compressibility Changes. As compared to previously studied workloads [14, 15, 17], the compressibility changes over time more often in GPU benchmarks. The most extreme example is 355.seismic, which begins with many zero values but slowly asymptotes to a 2x compression ratio over its execution. We also observe that although the overall compression ratio of the DL workloads stays roughly constant, there are frequent compressibility changes for individual memory entries. This is likely due to the fact that DL frameworks perform their own asynchronous GPU memory allocation with software-managed memory pools, and may reuse the same memory location for a variety of purposes over program execution [45]. In some cases, the data in a memory-entry can grow more random over time, thereby decreasing its compressibility. This would require more space to be allocated for the same memory-entry, causing a *memory-entry overflow*, and thereby additional data movement, as discussed in Section 2.4.

3.2 Buddy Compression Overview

Buddy Compression allows a programmer or DL framework to annotate the program such that they take up less device memory than the allocation size. For instance, if a user has 24GB of data and a GPU with only 12GB of memory capacity, the data can be allocated with a target of 2x compression. This means that only half of the full data size is allocated on the GPU device memory. We use compression to opportunistically fit data into this reduced device-resident allocation. If a memory-entry does not compress sufficiently, an NVLink-connected larger-but-slower memory is available as overflow storage. The *buddy-memory* is used as extended storage, with the data being striped across at 128B memory-entry granularity. Data from compressible memory-entries is sourced completely from GPU device memory, while incompressible memory-entries are sourced from both device and buddy-memory.

As shown in Figure 4, Buddy Compression stripes the data using 32B sectors. This 32B sector size is chosen to match the access granularity of GPU memory, specifically, GDDR5, GDDR5X, GDDR6, and HBM2-based GPUs. For example, if an allocation targets a compression ratio of 2x, the first two sectors per 128B memory-entry are mapped to device memory, while the last two are mapped to system memory. Therefore, if a memory-entry can be compressed by 2x or more, it fits completely in device memory, and otherwise, the rest of its data is saved in its fixed pre-allocated

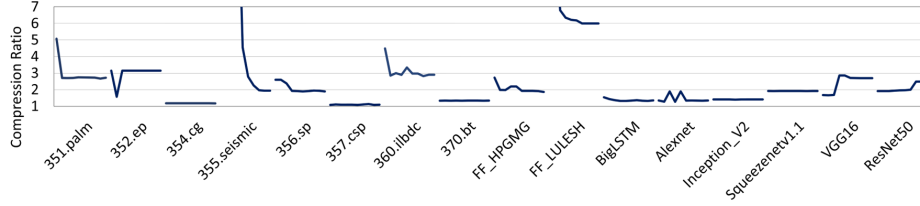


Fig. 3: The average compression ratio of the allocated memory for the complete run of each benchmark. Ten equally distributed memory-snapshots are taken during the entire run of each benchmark, and the compression ratio calculated.

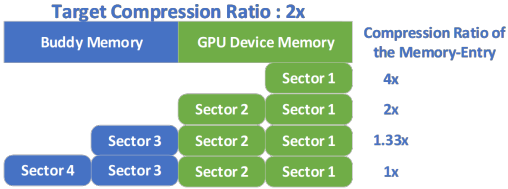


Fig. 4: Depending on its data, a 128B memory-entry compresses to occupy from 1-4 sectors of 32B each. Here, the target compression ratio is 2x. If an entry does not compress to 2x, left over sectors are accessed from buddy-memory.

spot in the buddy-memory. The allowed compression ratios for this study are 1x, 1.33x, 2x and 4x (4, 3, 2, or 1 sectors allocated in device memory). These ratios are chosen to keep the sector interleaving simple and avoid unaligned sector accesses.

Buddy-Memory Carve-Out Region. At boot time, the host system carves out a physically-contiguous chunk of its memory for each GPU, dedicating this storage to be used as each GPU’s buddy memory. Those regions are then never accessed by the host, eliminating any coherence issues. The buddy-memory size should correspond to the maximum target compression ratio for the GPU. As an example, if the maximum target compression ratio is 4x, then the carve-out region should be 3x as large as GPU device memory, in order to allow each memory-entry to have 3 sectors in host memory (in the worst case) and only 1 on the GPU.

Compression Metadata and Address Translation. Once the data is stored in compressed form, addressing it requires some additional translation and metadata. This metadata informs us about (i) the target compression ratio, (ii) whether or not a particular memory-entry was compressed to the target ratio, and (iii) the address in buddy-memory to be accessed for memory-entries that did not compress to the target ratio.

A global base address for the buddy-memory carve-out region is stored in a Global Buddy Base-address Register (GBBR). The page-table and TLBs are extended to store the information about whether the page is compressed or not, the target compression ratio, and the offset of buddy-page from the global base address. This adds a total overhead of 24 bits per page-table entry. To know the actual compressed size of each 128B memory-entry, there are 4 bits of metadata per cache block, stored in a dedicated region of device memory, amounting to a 0.4% overhead in storage. The metadata storage overheads of Buddy Compression are either comparable to, or less than those of previous works in memory compression in CPUs [13–17]. Figure 5a shows a very high-level view of the metadata setup and translation. The simple GBBR-offset based addressing makes the overall translation mechanism very simple.

A **metadata cache** is used to avoid additional memory accesses each time memory is accessed. Figure 5b shows the metadata cache

hit ratios as a function of the metadata cache size. Most applications have high hit ratios. We use a 4-way 64KB metadata cache, that is split into 8 slices, 1 per DRAM channel. Each metadata cache entry is 32B, thereby causing a prefetch of metadata corresponding 63 neighboring 128B memory-entries on every metadata cache miss. The metadata is assumed to be interleaved across the DRAM channels using the same hashing mechanism as regular physical-address interleaving.

3.3 Benefits of the Buddy Compression Design

No Page-Faulting Expense. The immense parallelism of a GPU increases the throughput of work done. Driver-based page-fault handling, however, is remote and non-distributed, making GPU page-faults during the runtime of a kernel very expensive [11]. As data is written back to memory, its compressibility can decrease, requiring new page allocations to store the same data. The page fault overhead in GPUs makes reducing the compressed data movement a very important directive. *The uniqueness of the design lies in the fact that the compressibility of each memory-entry affects only its own allocation, thereby never having to cause page movement.*

Low Translation Overhead. Memory bandwidth is a frequent bottleneck for GPUs. Accordingly, there has been fruitful research on bandwidth compression of GPU main memory [43, 46]. Buddy Compression uses compression to amplify *both* the bandwidth and capacity of GPU memory. However, as discussed earlier, compression-for-capacity requires additional metadata accesses for translation into the compressed address space. This makes reducing the metadata size and keeping translation simple important. Buddy Compression requires only 0.4% metadata, and since the carve-out region is contiguous in host memory, addressing into the buddy-memory is offset-based, and trivial.

No Impact on Small Workloads. If the available GPU device memory is enough to allocate the memory required by the application, the Buddy Compression can be disabled. In that case, the design does not affect the performance at all.

3.4 Reducing Buddy Compression Overheads

With the design of Buddy Compression, the obvious overhead comes from having to access the slower buddy-memory in cases of unexpectedly low compression.

Profiling for Target Compression Ratio. Choosing the right target compression ratio is important, since aggressive compression ratios will lead to more memory-entries exceeding the allocated device memory and requiring buddy-memory accesses. To choose the target compression ratio, we use a simple profiling pass on a representative dataset. For HPC workloads, the profiling pass is run using a smaller dataset, like the train dataset for SpecAccel2.

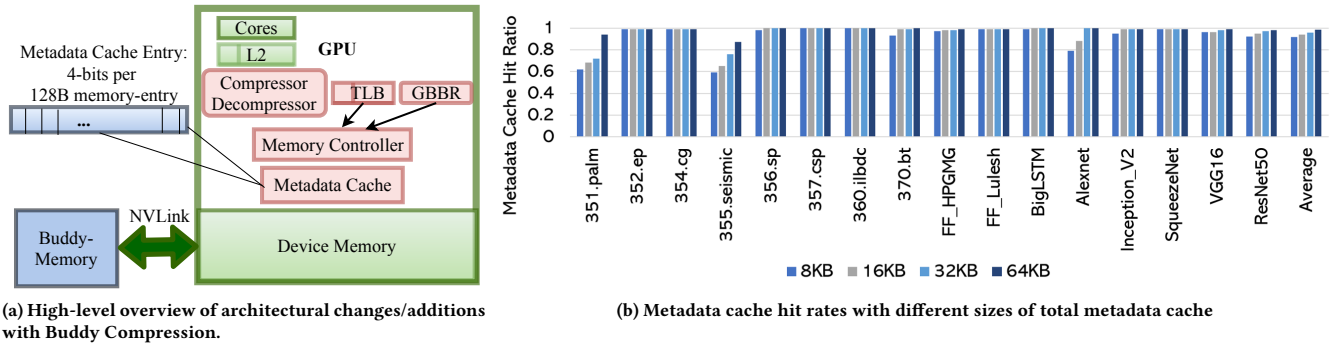


Fig. 5: Compression metadata handling and architecture

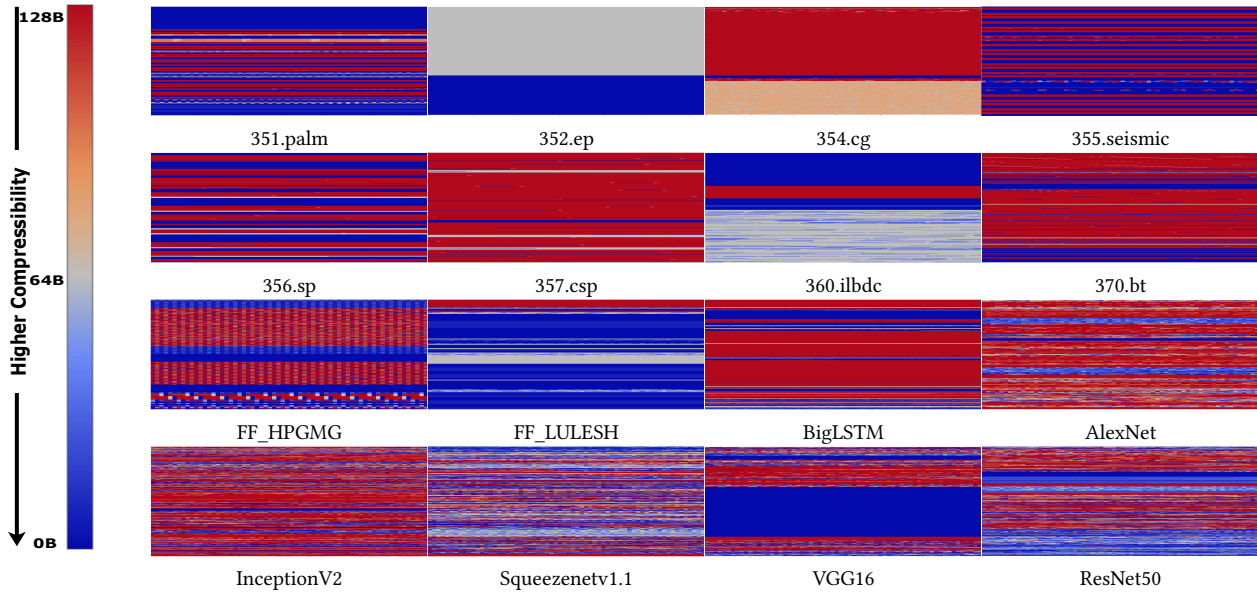


Fig. 6: Spatial patterns of compressibility. Each plot is a heatmap of compressibility per 128B memory-entry for the allocated GPU memory. Each horizontal line is an 8KB page and pages are stacked vertically as per address.

For DL workloads, this profiling pass is run with a smaller batch size, and can be embedded in the training platform, like PyTorch or TensorFlow. Furthermore, the target ratios can be periodically updated for long running applications, e.g., for DL training, the target ratio update can be combined with checkpointing in the framework. In this paper, for simplicity, we consider a single static target compression ratio throughout the run of the application.

Annotation Granularity. The granularity with which the programmer annotates memory is also important—the best annotation granularity depends on the spatial characteristics of compressibility. Naive Buddy Compression considers a single, conservative target compression ratio for the whole-program. As shown in Figure 7, we find this granularity to be too coarse. The naive mechanism achieves an overall compression ratio of 1.57x for HPC workloads, and 1.18x for DL workloads, with 8% accesses over the interconnect to the buddy-memory for HPC, and 32% for DL. The overall compression is low, and, given that even the highest available bandwidth on the interconnect (NVLink2, 150GBps) is 6x lower than the GPU device memory bandwidth (900GBps), the overheads from these buddy-memory accesses are high. The

desirable solution for us would be something that effectively lowers the buddy-memory accesses, while maintaining high compression ratios. In order to find such a solution, we present a deep dive into the detailed compression data patterns in these workloads.

Understanding Compressibility Patterns. Figure 6 shows a spatial plot (in the virtual address space) of the compressibility of each workload’s data. Each sub-plot is a spatial heat map that shows the compressibility of each 128B memory-entry in the memory allocated by each benchmark. A colder color (blue), signifies high compressibility and hotter color (red) shows low compressibility. The plot is structured assuming 8KB pages, where each page has 64 128B memory-entries laid along x-axis. The y-axis is the total number of pages in the memory of the benchmark. Figure 6 shows that the spatial locality of compressibility of data varied significantly across benchmarks. While most HPC benchmarks have large homogeneous regions of similar compressibility, the distribution is more random in DL workloads. FF_HPGMG shows specific patterns of compressibility that can directly be correlated with the arrays of heterogeneous structs that are used in its allocation. Although the DL workloads do not show the level of homogeneity

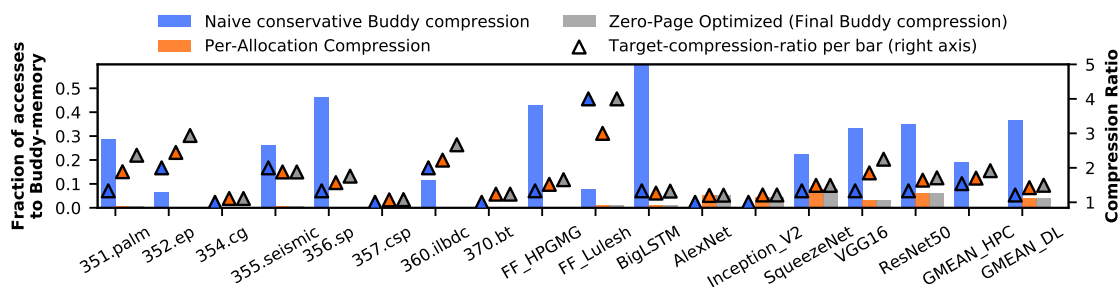


Fig. 7: Sensitivity of the compression ratio and buddy-memory accesses to design optimizations.

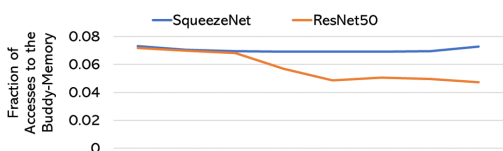


Fig. 8: The fraction of buddy storage accesses over the execution of one iteration in DL training. We achieve a constant compression ratio of 1.49 for SqueezeNet and 1.64 for Resnet.

that can be seen in HPC workloads, there are still some mostly-red or mostly-blue regions. Based on the insights from these plots, we propose optimizations to the design of Buddy Compression.

Per-Allocation Compression Targets. Figure 6 shows that there are several regions that are mostly-red, or mostly-blue. We find that the majority of these region boundaries overlap with `cudaMalloc()` boundaries. A special allocation API for compressed regions allows us to capture this behavior and eliminate the futile effort of compressing the red regions.

During profiling, we periodically take snapshots of memory, to track the compression ratios per allocation. At the end of profiling, we decide target compression ratios per allocation using heuristics to trade-off the compression ratio with the buddy-memory accesses. The compression ratio chosen is conservative to minimize the buddy-memory accesses. As an example, based on Figure 3, for 355.seismic, for most allocations, the target ratio used will be 2x, and not 7x or 6x. We use a static target compression ratio for the entire run of the application. This is because a dynamic target compression ratio would require reallocating and moving around the pages, making the compression management more complicated and less performant, unless the applications are very long running and the overheads are amortized.

Buddy Threshold. Most benchmarks have regions that are highly homogeneous in their compressibility, making the per-allocation target ratio decision simple. However, for benchmarks like AlexNet and ResNet50, the regions are mixed in compressibility. Therefore, target compression ratio decision in these cases, involve a trade-off between compression ratio and buddy-memory accesses. We define a Buddy Threshold, that sets a limit on the fraction of memory-entries that require accessing the buddy-memory, per-allocation. A higher Buddy Threshold achieves a higher compression ratio at the cost of more buddy-memory accesses, and hence, lower performance. These buddy-memory accesses are calculated per target compression ratio, using a histogram of the static memory snapshots.

Figure 9 shows the results from a sensitivity study of the Buddy Threshold (10% to 40%). In addition to this, the figure shows the best achievable compression ratio assuming no constraints are placed on the buddy-memory accesses. The bars in the figure show that the buddy-memory accesses remain very low for HPC benchmarks, due to their homogeneous regions. For DL benchmarks however, the buddy-memory accesses are more frequent, and increase further as the buddy threshold is increased. Similarly, the compression benefits from increasing the buddy threshold are mostly seen in DL benchmarks. With the exception of FF_HPGMG, we are able to achieve near-optimal compression, as can be seen in comparison with the black marker. FF_HPGMG, as discussed earlier has a peculiar striped compressibility pattern resulting from the struct it uses. To capture the maximum compression, FF_HPGMG requires more than 80% Buddy Threshold for most of its allocated memory region. Another interesting scenario is seen in benchmarks 354.cg and 370.bt. Since these benchmarks mostly consist of incompressible data, without the per-allocation targets, Buddy Compression was unable to compress them at all. However, with the per-allocation targets, we are able to compress them by 1.1x and 1.3x respectively. Overall, since a 30% Buddy Threshold achieves a good balance between the compression and buddy-memory accesses, we choose this for our final Buddy Compression design.

Since the target compression ratio remains constant, while actual data compressibility can change over time, these statically calculated buddy-memory accesses may not be similar across the run. To investigate this, we observed the buddy-memory accesses across all the memory dumps, while maintaining constant target compression ratios. Figure 8 presents the results from ResNet50 and SqueezeNet, both of which have frequent changes in compression ratio per memory-entry, and have high accesses to buddy-memory to begin with. We observe that the buddy-memory accesses do not change a lot over time. This is because even though the individual memory-entries frequently change their compressibility, the changes are almost equal in both directions, making the overall effects small. Furthermore, as mentioned earlier, for benchmarks that see large changes in their overall compressibility, like 355.seismic, we avoid this challenge by choosing conservative target compression ratios.

Special Case For Mostly-Zero Allocations. Based on the spatial plots, we observe that there are areas in memory that remain mostly-zero even across complete benchmark executions. To capture the capacity-expanding opportunity of such allocations, we add an aggressive target compression ratio of 16x where we keep only

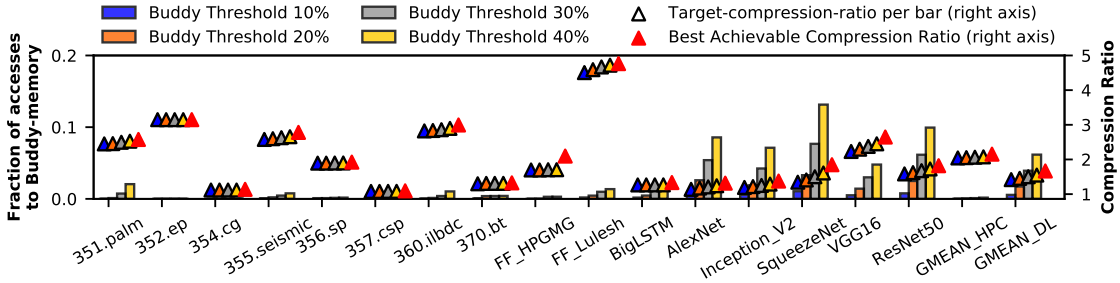


Fig. 9: Sensitivity of the compression ratio and buddy-memory accesses to the Buddy Threshold parameter.

8B out of each 128B in device memory. Note that the only change involved here is an additional encoding for page size in the TLB.

This optimization allows us to increase the compression ratio for benchmarks with large highly-compressible regions, for example, 352.ep, and VGG16. Note that this optimization does not have much impact on the buddy-memory accesses, since such compressible data would always fit in device memory. Figure 7 shows the impact of this optimization. For HPC benchmarks, the compression ratio goes up from 1.7x to 1.9x, while for DL, from 1.42x to 1.5x.

For this optimization, it is important to identify allocations that are mostly zero, and remain so for the entirety of the run of the benchmark, unless there is a periodic update of target compression ratio. The profiler marks the regions that can be compressed with this optimization, such that the overall compression ratio is still under 4x, limited by the buddy-memory carve-out region.

Possible Optimization for Metadata Access. We note that on a metadata cache miss, both the device-memory data and its metadata can be accessed in parallel, since the metadata only informs us about the buddy-memory part of data. We do not, however access the buddy-memory in parallel, since the buddy-memory accesses are rare on average (Figure 7).

3.5 Final Design

Buddy Compression uses a Buddy Threshold default of 30%, a metadata cache of 4KB per DRAM channel, and a buddy-memory region of size 3x of the GPU device memory, to support a 4x maximum compression ratio. The application is first profiled with a smaller dataset, during which our tool periodically calculates a histogram of compressed memory-entries per allocation. At the end of profiling, the tool reports the target compression ratios, which are then used by the DL platform, or the HPC user to annotate cudamalloc API calls, enabling running a larger dataset without the overheads of Unified Memory. Figure 7 shows the compression ratio and buddy-memory accesses for the final design. We achieve 1.9x compression for HPC and 1.5x compression for DL workloads. The average buddy-memory accesses are 0.08% for HPC and 4% for DL workloads.

4 PERFORMANCE EVALUATION

We have already presented results regarding buddy-memory accesses and compression ratios from Buddy Compression in Figure 7. In this section, we first discuss the performance impact of Buddy Compression relative to an ideal large-capacity GPU, followed by a comparison to UM-based oversubscription. We then

Tab. 2: Performance simulation parameters.

Core	1.3 GHz; 2 greedy-then-oldest warp schedulers per SM Max 64 32-thread warps per SM
Caches	24KB private L1/texture cache per SM, 128B lines 64KB dedicated scratchpad per SM, 4MB shared L2, 32 slices, 128B lines, 16 ways
Off-Chip	32 HBM2 channels at 875MHz (900 GBps) 6 NVLink2 bricks (150 GBps full-duplex*)
Buddy	4KB ¹ metadata cache per L2 slice, 128B lines, 4 ways Compression/Decompression latency = +11 cycles

* These parameters are swept in later parts of the evaluation.

present a case-study of DL training to estimate the performance benefits from increased capacity.

4.1 Methodology

Workloads. As previously described, we evaluate Buddy Compression’s effectiveness on workloads from the SpecAccel [47] and FastForward benchmark suites for HPC workloads. We collect a representative trace from each benchmark while running the reference datasets. Each trace contains 1–9 billion warp instructions and corresponds to the dominant kernel of each benchmark at a point in execution that exhibits the average compression ratio for that entire benchmark execution [48]. For DL, we use a set of 5 convolutional neural networks: AlexNet [49], Inception v2 [50], SqueezeNetv1.1 [51], VGG16 [52], and ResNet50 [53], all of which were run under the Caffe [45] framework with the ImageNet [54] dataset. Additionally we consider a long short-term memory network, BigLSTM [55], which is a 2-layer LSTM with a 8192+1024 dimensional recurrent state in each of the layers and uses the English language model. The traces for the DL training workloads span one full training iteration.

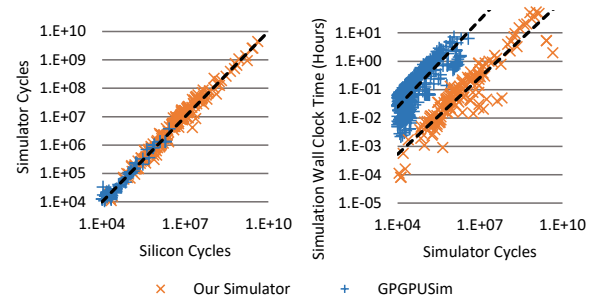


Fig. 10: Our simulator correlates with a V100 GPU (left, with slope=1 line). It is two orders of magnitude faster than GPGPUSim [56], enabling longer programs (right, linear regression lines).

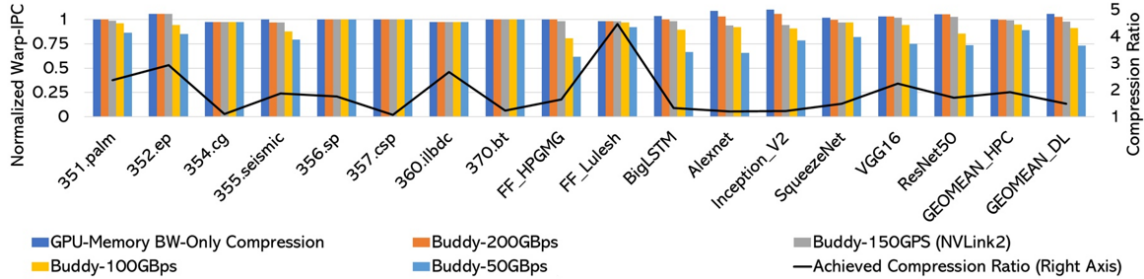


Fig. 11: The performance impact of compression, not accounting for capacity benefits. Systems with different link bandwidths are evaluated (showing unidirectional full-duplex bandwidths), with results normalized to a system with unlimited memory and a 150GBps interconnect.

Simulation Infrastructure. We use a dependency-driven GPU performance simulator, similar to the one used by Arunkumar et al. and others [57–59]. We configure the simulator based on publicly information about NVIDIA’s P100 Pascal GPU [60] and the interconnect characteristics of recent Volta GPUs [61] (Tab. 2). Non-public microarchitectural details are configured using microbenchmark results from Jia et al. [44]. Each SM is modeled as an in-order processor with greedy-then-oldest warp scheduling. We model a multi-level cache hierarchy with private L1 caches and a shared sectored L2 cache with 128B lines and 32B sectors. Caches are banked to provide the necessary parallelism to saturate DRAM bandwidth. We model software-based cache coherence in the private caches, similar to state-of-the-art GPUs. The memory system consists of 32 HBM2 channels and the GPU is connected to the system with 6 NVLink2 bricks.

We conservatively model decompression latency as 11 DRAM cycles, as discussed in prior work [43]. Unless explicitly noted, the default metadata cache configuration is 4-way set associative 4KB per L2 slice. Additionally, to separate out its performance impact, we also evaluate bandwidth-only interconnect compression between the L2 cache and device memory. Such compression does not increase the effective memory capacity, but it can increase the bandwidth between L2 cache and memory without requiring any metadata or buddy-memory accesses.

Figure 10 (left) shows that our simulator correlates well (correlation coefficient 0.989) against the total cycles spent on a real V100 GPU across a wide variety of benchmarks across a number of domains.¹ Corresponding numbers from GPGPUSim (correlation coefficient 0.948), a widely-used academic simulator, are also shown. Our motivation in using a proprietary simulator comes from the two orders-of-magnitude speed benefit shown in Figure 10 (right), which enables us to simulate larger and more realistic workloads.

4.2 Performance Relative to an Ideal GPU

Apart from increasing the memory capacity, Buddy Compression can affect the performance of the system in the following ways: (i) Buddy-memory accesses can cause a performance hit. (ii) Decompression latency can hinder performance. (iii) Metadata cache misses can cause additional requests to device memory. (iv) It has two conflicting effects on the effective bandwidth from L2 cache to device memory. First, since compression is done at the cache-block

granularity, the minimum L2 fill granularity is no longer a single 32B sector. Instead, the complete cache-block is transferred to L2 upon a load access to a compressed memory-entry. This may result in over-fetch for fine-grained accesses, squandering device memory bandwidth. However, for compressible workloads with high locality, compression allows an increase in effective bandwidth because cache-blocks can be fetched with fewer memory accesses.

We evaluate Buddy Compression alongside bandwidth-only compression that compresses the data being transferred between L2 cache and device memory. We also sweep the buddy-memory interconnect bandwidth from 50 to 200GBps on full-duplex connection, where 150GBps represents NVLink2. The results are shown in Figure 11. Bandwidth-only compression achieves an overall speedup of 5.5%. Most of this speedup comes from the DL training workloads. This is because of the regular, streaming memory accesses of these workloads, which are essentially performing matrix multiplications. Since most of their memory accesses are coalesced to access all sectors in each cache-block, bandwidth compression achieves higher effective bandwidth by requiring fewer packets per request. On the other hand, the HPC applications 354.cg and 360.ilbdc experience slowdowns with bandwidth compression. This is because of the random and irregular memory access pattern of these benchmarks. Most of their memory accesses require only one sector. However, bandwidth compression leads to a full cache-block transfer of any compressible data, potentially lowering the effective bandwidth for random accesses. FF_Lulesh experiences a slowdown despite having a regular memory access pattern. We find the reason behind this to be the compression and decompression latency, which both lie on the critical path for bandwidth compression.

Buddy Compression introduces additional overheads on top of bandwidth compression, in the form of metadata cache misses and buddy-memory accesses. Figure 11 shows that while an interconnect bandwidth of 200GBps still achieves a 2% average speedup using Buddy Compression, all lower interconnect bandwidths experience some slowdown relative to the ideal large-capacity GPU that serves as the baseline. Note that the performance benefits from a larger memory capacity are not accounted for in these experiments.

The benchmarks 351.palm and 355.seismic experience slowdown due to a higher metadata cache miss rate, as can be seen from Figure 5b. Since the other benchmarks have high metadata cache hit rates, metadata accesses do not have a discernible impact on their performance.

Most HPC benchmarks have rare buddy-memory accesses (Figure 7), leading to negligible slowdowns with a high bandwidth

¹We show simulator correlation results with a slightly different configuration than is used for evaluation, in order to also be able to show comparable GPGPUSim results. The P100 configuration used in the paper also correlates well with silicon.

interconnect. However, when the interconnect bandwidth is reduced, even these 1% accesses from buddy-memory can cause a considerable slowdown of bandwidth-sensitive applications like 352.ep and 355.seismic. Note that FF_HPGMG has host-memory accesses in its native form, due to synchronous copies from host to device. Therefore, lowering the link bandwidth shows a drastic impact on its performance (since all results are normalized to a baseline system without compression and a 150 GBps interconnect).

DL training workloads have a higher percentage of buddy-memory accesses, as can be seen in Figure 7. These buddy-memory accesses are caused by a lack of compression locality in the workloads. For example, AlexNet requires accesses to 5.4% of memory locations to go to buddy-memory, leading to a 6.5% slowdown relative to ideal (with a 150GBps full-duplex interconnect). This is because of the difference in the bandwidth available from device memory vs. buddy-memory, which in our setup is 900GBps and 150GBps. Performance degenerates quickly as this disparity grows, with the 50GBps full-duplex connection seeing a 35% slowdown.

These results show that recently-developed high-speed GPU interconnects are an enabling technology for Buddy Compression. The slowest link we evaluate (50 GBps full-duplex) is still faster than the most recent PCIe generation (x16 PCIe4.0, providing 32GBps full-duplex bandwidth) yet it suffers from more than 20% average slowdown relative to the ideal GPU. However, using high bandwidth interconnects such as NVLink2 (150Gbps full-duplex) enables Buddy Compression to come within 1% of the performance of the large-capacity GPU on HPC benchmarks, and within 2.2% of ideal on DL training workloads.

4.3 Comparison with Unified Memory

Faithfully comparing the performance of Buddy compression to Unified Memory in simulation is not feasible due to the complex host-driver interactions and page migration policies implemented within UM. Instead we choose to understand UM performance in oversubscription scenarios on real hardware. Figure 12 shows measured performance of three applications on an IBM Power9 system, connected to a Tesla V100 GPU via NVLink2 (3 bricks, 75 GBps full-duplex bandwidth). We use SpecAccel applications with the *managed* PGI compiler flag, and force varying levels of oversubscription through an interposer that hogs GPU memory at application startup. We also run the applications using a compiler flag to pin all allocations in host memory, showing the slowdown in dotted lines. Our results indicate that UM migration heuristics often perform worse than running applications completely pinned in host memory; perhaps because UM was primarily intended for the ease of programming and has not yet been tuned for high-performance memory oversubscription. Previous work [11, 31] supports our observation that the slowdown due to UM oversubscription can be excessive without more extensive hardware support. Figure 11 shows that Buddy Compression suffers from at most 1.67x slowdown for these programs when oversubscribing by 50%, even with a conservative 50 GBps NVLink speed. This indicates that it is a better alternative to high performance memory over subscription than software-based UM.

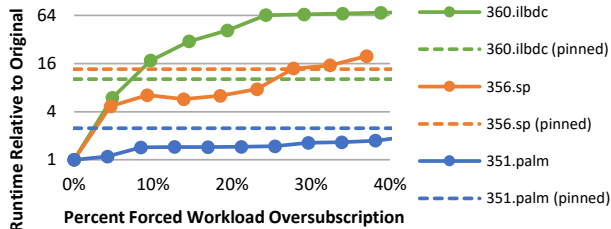


Fig. 12: Measured overheads of using UM oversubscription. A Power9 CPU is connected via 3 NVLink2 bricks (75 Gbps full-duplex) to an NVIDIA V100 GPU. Dotted lines show the performance when all allocations are in the host memory.

4.4 Case Study: DL Training Benefits from Increased Memory Capacity

Thus far, we have compared the performance of Buddy Compression to an uncompressed, large-memory baseline (Figure 11). This excludes the benefits of having access to a larger-memory, thus ignoring the main purpose of Buddy Compression. In the case of HPC benchmarks, a larger memory enables solving a larger problem. Such benefits are important yet difficult to quantify. Accordingly, we instead perform a case-study on DL training workloads to quantify the performance benefits from compression.

Stochastic Gradient Descent (SGD) is widely used to update weight values during DL network training. SGD iterates repeatedly through the training dataset, optimizing and updating the model each iteration. Updates depend on hyperparameters (such as the chosen learning rate) and dynamically react as the classification accuracy increases. The entire dataset is divided into mini-batches, and each iteration goes through one mini-batch and updates the model. While there is an ongoing debate concerning the utility of large mini-batches across all domains, they can help regularize and improve convergence in many cases, as evidenced by [3, 5].

Memory Footprints of DL Workloads. The memory footprint of a network during training depends on the mini-batch size. Larger mini-batch sizes require a larger part of the dataset to reside in device memory, along with more intermediate data (activations and gradients). Figure 13a shows the memory footprint of each of our DL training workloads as the mini-batch size is increased. The sizes are increased up to the maximum size that a Titan Xp GPU can support (12GB device memory). Initially there is not much difference as the batch size is doubled. Eventually, however, the memory footprint grows almost linearly with increasing mini-batch size. This transition point depends on the size of the network parameters, which do not vary with mini-batch size. For example, for AlexNet, the network parameters are a large portion of the overall memory consumption due to the three large fully-connected layers and relatively few (five) convolutional layers. This leads to a later transition point for AlexNet at a batch-size of 96; all other tested networks transition to an increasing memory footprint at a batch size of 32 or below.

Performance Impact of Larger Mini-Batches. A larger batch size is beneficial for DL training [3, 55], because it allows more work to be done per iteration, leading to higher resource utilization. We use an analytical model very similar to [62, 63] to project this, since we cannot collect traces for DL execution with memory capacity requirements that are larger than current GPU’s capacity. We extensively validate the model and its projections highly

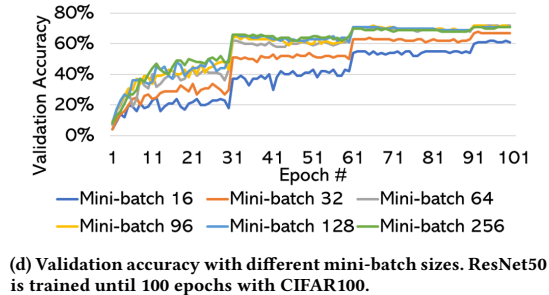
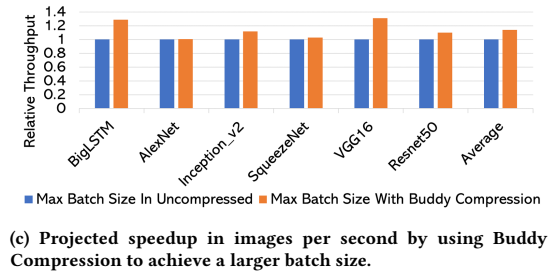
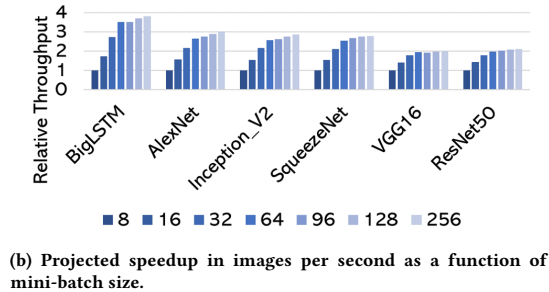
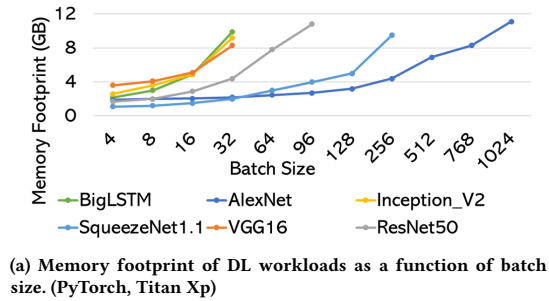


Fig. 13: Impact of increasing mini-batch size on DL training

correlate with a range of existing commercial GPUs. Figure 13b shows the projected speedup for each network as the mini-batch size is increased. It is generated using a detailed analytical model of deep learning training efficiency (Section 4.1). As shown in the figure, increasing the mini-batch size leads to higher speed in terms of frames per second. This effect, however, is only seen until the mini-batch size is large enough to utilize most of the GPU resources. After the point of full GPU utilization, the effect plateaus.

Buddy Compression allows us to fit a larger mini-batch into GPU memory. Figure 13c shows the relative speedup projected by our model for this larger mini-batch size over a baseline GPU

with 12GB of device memory. The average speedup is 14%, while individual workloads like BigLSTM and VGG16 achieve high speedups of 28% and 30%, respectively. The reason for the higher speedup in these workloads follows from Figures 13a and 13b. Without compression, both of these are unable to fit the mini-batch size of 64, which needed for good resource utilization.

This overall speedup of 14% is much higher than the 2.2% performance overhead due to Buddy Compression (Figure 11). This indicates that Buddy compression can lead to significant performance gain for capacity-constrained GPUs by allowing the use of larger mini-batch sizes.

Better Convergence with Larger Mini-Batches. Apart from improving computational throughput with better resource utilization, the mini-batch size can also impact the training accuracy. In order to investigate this, we train ResNet50 on the CIFAR100 [64] dataset for 100 epochs on a Titan Xp GPU with different mini-batch sizes. Figure 13d shows the validation accuracy results for these runs. As can be seen, very small mini-batches of 16 and 32 do not reach the maximum accuracy, despite using the corresponding, tuned hyperparameters. Additionally, although the mini-batch size of 64 trains to the maximum accuracy, it converges slower than the larger mini-batches. With batch normalization, the jitter in the accuracy is also higher with small mini-batch sizes. While we observe good validation accuracy up to a batch size of 256, which is in line with the reported results in previous work [3], it has been reported that increasing the mini-batch beyond a certain size can be detrimental to the network’s generalization. However, there has been other work on tuning loss functions and hyperparameters for successful training with large mini-batches [65, 66].

Huge DL Networks. Recent object detection networks like MegDet [3] and natural language processing networks like BERT [5] are unable to fit more than 2-4 input samples per GPU during training, due to memory capacity limits. This is a hurdle for developers, since the best regularization technique, Batch Normalization requires a batch size of at least 32 samples to be effective [67]. As a result, developers resort to horizontal scaling by spreading a mini-batch across many GPUs. As an example, the version of MegDet that won the COCO challenge [68] in 2017, performs batch normalization across 128 GPUs, resulting in high communication overhead. They also present results proving that larger mini-batches lead to higher accuracy, and are faster to train. Using horizontal scaling alone to support larger batches is not sustainable due to the inter-GPU communication bottleneck. While our simulation infrastructure is unable to support such huge DL training networks, Buddy Compression enables modest vertical scaling, which, when combined with horizontal scaling can lead to more sustainable solutions.

The final takeaway from this case-study is that most DL networks require a mini-batch of at least 64 or 128 in order to achieve near-maximum throughput and best accuracy (with batch normalization). Buddy Compression can help achieve the required mini-batch sizes for large networks using fewer GPUs.

5 CONCLUSIONS

This work proposes and evaluates Buddy Compression: the first general-purpose mechanism that can be used to increase user visible GPU memory capacity on GPUs. Buddy Compression

is enabled by modern high-bandwidth interconnects that allow remote memory pool to be used as a backup when the compressibility is not sufficient. Buddy Compression is able to achieve 1.5–1.9× memory compression ratios across a wide range of HPC and deep learning workloads while incurring only a 1–2% performance penalty compared to a system with a larger GPU memory capacity, due to its unique design where compressibility changes do not incur additional data movement. This combination of high performance and reasonable compression ratios makes Buddy Compression an attractive and performant alternative to existing technologies like Unified Memory oversubscription.

REFERENCES

- [1] L. Gu, J. Siegel, and X. Li, “Using GPUs to Compute Large Out-of-card FFTs,” in *Proceedings of the International Conference on Supercomputing*, ser. ICS ’11, 2011.
- [2] F. Song, S. Tomov, and J. Dongarra, “Enabling and scaling matrix computations on heterogeneous multi-core and multi-gpu systems,” in *Proceedings of the 26th ACM International Conference on Supercomputing*, ser. ICS ’12, 2012.
- [3] C. Peng, T. Xiao, Z. Li, Y. Jiang, X. Zhang, K. Jia, G. Yu, and J. Sun, “Megdet: A large mini-batch object detector,” *CoRR*, vol. abs/1711.07240, 2017.
- [4] X. Chen, D. Z. Chen, and X. S. Hu, “moDNN: Memory optimal DNN training on GPUs,” in *Proceedings of the Conference on Design, Automation, and Test in Europe (DATE)*, Mar. 2018, pp. 13–18.
- [5] J. Devlin, M.-W. Chang, K. Lee, and K. Toutanova, “BERT: Pre-training of Deep Bidirectional Transformers for Language Understanding,” *CoRR*, vol. abs/1810.04805, 2018.
- [6] M. Wang, C.-c. Huang, and J. Li, “Supporting Very Large Models using Automatic Dataflow Graph Partitioning,” *arXiv:1807.08887 [cs]*, Jul. 2018.
- [7] T. Akiba, T. Kerola, Y. Niitani, T. Ogawa, S. Sano, and S. Suzuki, “PFDet: 2nd Place Solution to Open Images Challenge 2018 Object Detection Track,” *arXiv:1809.00778 [cs]*, Sep. 2018.
- [8] M. Rhu, N. Gimelshein, J. Clemons, A. Zulfiqar, and S. W. Keckler, “vDNN: Virtualized Deep Neural Networks for Scalable, Memory-efficient Neural Network Design,” in *Proceedings of the International Symposium on Microarchitecture (MICRO)*, 2016, pp. 18:1–18:13.
- [9] M. Rhu, M. O’Connor, N. Chatterjee, J. Pool, Y. Kwon, and S. W. Keckler, “Compressing DMA Engine: Leveraging Activation Sparsity for Training Deep Neural Networks,” in *Proceedings of the International Symposium on High Performance Computer Architecture (HPCA)*, Feb. 2018, pp. 78–91.
- [10] M. Harris. (2016) Unified memory for CUDA beginners. NVIDIA Blog. [Online; accessed 18-Jan-2018].
- [11] T. Zheng, D. Nellans, A. Zulfiqar, M. Stephenson, and S. W. Keckler, “Towards high performance paged memory for gpus,” in *2016 IEEE International Symposium on High Performance Computer Architecture (HPCA)*. IEEE, 2016.
- [12] Ammar Ahmad Awan, Ching-Hsiang Chu, Hari Subramoni, Xiaoyi Lu, and Dhableswar K. Panda, “Can Unified-Memory support on Pascal and Volta GPUs enable Out-of-Core DNN Training?”
- [13] R. B. Tremaine, P. A. Franaszek, J. T. Robinson, C. O. Schulz, T. B. Smith, M. Wazlowski, and P. M. Bland, “IBM Memory Expansion Technology (MXT),” in *IBM Journal of Research and Development*, vol. 45, no. 2, 2001.
- [14] M. Ekman and P. Stenstrom, “A Robust Main-Memory Compression Scheme,” in *Proceedings of the 32nd Annual International Symposium on Computer Architecture*, 2005.
- [15] G. Pekhimenko, V. Seshadri, Y. Kim, H. Xin, O. Mutlu, P. Gibbons, M. Kozuch, and T. Mowry, “Linearly compressed pages: a low-complexity, low-latency main memory compression framework,” in *Proceedings of the 46th Annual IEEE/ACM International Symposium on Microarchitecture*, 2013.
- [16] J. Zhao, S. Li, J. Chang, J. L. Byrne, L. L. Ramirez, K. Lim, Y. Xie, and P. Faraboschi, “Buri: Scaling Big-Memory Computing with Hardware-Based Memory Expansion,” *ACM Trans. Archit. Code Optim.*, vol. 12, no. 3, 2015.
- [17] E. Choukse, M. Erez, and A. R. Alameldeen, “Compresso: Pragmatic Main Memory Compression,” in *Proceedings of the International Symposium on Microarchitecture (MICRO)*, 2018.
- [18] J. Nystad, A. Lassen, A. Pomianowski, S. Ellis, and T. Olson, “Adaptive scalable texture compression,” in *Proceedings of the Fourth ACM SIGGRAPH / Eurographics Conference on High-Performance Graphics*, ser. EGGH-HPG ’12, 2012.
- [19] A. Jain, A. Phanishayee, J. Mars, L. Tang, and G. Pekhimenko, “Gist: Efficient Data Encoding for Deep Neural Network Training,” in *Proceedings of the International Symposium on Computer Architecture (ISCA)*, Jun. 2018, pp. 776–789.
- [20] NVIDIA. NVIDIA DGX-2: The world’s most powerful AI system for the most complex AI challenges. <https://www.nvidia.com/en-us/data-center/dgx-2/>.
- [21] O. Consortium. OpenCAPI 3.0 Data Link Specification. [Online]. Available: <https://opencapi.org/wp-content/uploads/2016/09/OC-DL-Specification.10.14.16.pdf>
- [22] “Intel Hints Towards An Xe Coherent Multi-GPU Future With CXL Interconnect.” [Online]. Available: <https://wccftech.com/intel-xe-coherent-multi-gpu-cxl/>
- [23] L. Liu, L. L. Deng, X. Hu, M. Zhu, G. Li, Y. Ding, and Y. Xie, “Dynamic sparse graph for efficient deep learning,” *CoRR*, vol. abs/1810.00859, 2018.
- [24] A. Gruslys, R. Munos, I. Danihelka, M. Lanctot, and A. Graves, “Memory-efficient backpropagation through time,” in *NIPS*, 2016.
- [25] M. Rhu, N. Gimelshein, J. Clemons, A. Zulfiqar, and S. W. Keckler, “vDNN: Virtualized deep neural networks for scalable, memory-efficient neural network design,” *2016 49th Annual IEEE/ACM International Symposium on Microarchitecture (MICRO)*, pp. 1–13, 2016.
- [26] C. D. Sa, M. Leszczynski, J. Zhang, A. Marzoev, C. R. Aberger, K. Olukotun, and C. Ré, “High-accuracy low-precision training,” *CoRR*, vol. abs/1803.03383, 2018.
- [27] Y. Ito, R. Matsumiya, and T. Endo, “ooc_cudnn: Accommodating convolutional neural networks over GPU memory capacity,” in *2017 IEEE International Conference on Big Data (Big Data)*, Dec. 2017, pp. 183–192.
- [28] NVIDIA. NVIDIA Turing GPU Architecture. [Online]. Available: <https://www.nvidia.com/content/dam/en-zz/Solutions/design-visualization/technologies/turing-architecture/NVIDIA-Turing-Architecture-Whitepaper.pdf>
- [29] N. Sakharykh. (2017) Unified memory on pascal and volta. GPU Technology Conference (GTC). [Online]. Available: <http://on-demand.gputechconf.com/gtc/2017/presentation/s7285-nikolay-sakharykh-unified-memory-on-pascal-and-volta.pdf>
- [30] “zram: Compressed RAM based block devices.” 2012. [Online]. Available: <https://www.kernel.org/doc/Documentation/blockdev/zram.txt>
- [31] N. Sakharykh. (2016, December) Beyond gpu memory limits with unified memory on pascal. [Online]. Available: <https://devblogs.nvidia.com/beyond-gpu-memory-limits-unified-memory-pascal/>
- [32] —. (2018, March) Everything you need to know about unified memory. <http://on-demand.gputechconf.com/gtc/2018/presentation/s8430-everything-you-need-to-know-about-unified-memory.pdf>. GPU Technology Conference (GTC).
- [33] “Heterogenous System Architecture (HSA).” [Online]. Available: <https://www.hsafoundation.com>
- [34] “AMD Kaveri: Support for Heterogenous System Architecture (HSA).” [Online]. Available: <http://www.amd.com/en-us/products/processors/desktop/a-series-apu>
- [35] Tiffany Trader. (2017) TSUBAME3.0 points to future HPE Pascal-NVLink-OPA server. <https://www.hpcwire.com/2017/02/17/tsubame3-0-points-future-hpe-pascal-nvlink-opa-server/>. HPC Wire.
- [36] A. Caldeira. (2018, March) Ibm power system ac922 introduction and technical overview. [Online]. Available: <https://www.redbooks.ibm.com/redpapers/pdfs/redp5472.pdf>
- [37] P. Markthub, M. E. Belviranli, and S. S. Lee, J. S. Vetter, “DRAGON: Breaking GPU Memory Capacity Limits with Direct NVM Access,” in *Proceedings of the International Conference on High Performance Computing, Networking, Storage and Analysis (SC)*, 2018.
- [38] K. Lim, J. Chang, T. Mudge, P. Ranganathan, S. K. Reinhardt, and T. F. Wenisch, “Disaggregated memory for expansion and sharing in blade servers,” in *Proceedings of the International Symposium on Computer Architecture (ISCA)*, 2009.
- [39] G. Pekhimenko, V. Seshadri, O. Mutlu, P. Gibbons, M. Kozuch, and T. Mowry, “Base-Delta-Immediate Compression: Practical Data Compression for On-Chip Caches,” in *Proceedings of the International Conference on Parallel Architectures and Compilation Techniques (PACT)*, 2012.
- [40] A. R. Alameldeen and D. A. Wood, “Frequent Pattern Compression: A significance-based compression scheme for L2 caches,” Technical Report 1500, Computer Sciences Department, University of Wisconsin-Madison, Tech. Rep., 2004.
- [41] J. Yang, Y. Zhang, and R. Gupta, “Frequent value compression in data caches,” in *Proceedings of the 33rd Annual IEEE/ACM International Symposium on Microarchitecture*, 2000.
- [42] X. Chen, L. Yang, R. Dick, L. Shang, and H. Lekatsa, “C-PACK: A High-Performance Microprocessor Cache Compression Algorithm,” in *IEEE Educational Activities Department vol. 18*, 2010.
- [43] J. Kim, M. Sullivan, E. Choukse, and M. Erez, “Bit-Plane Compression: Transforming Data for Better Compression in Many-Core Architectures,” in *Proceedings of the 43rd Annual International Symposium on Computer Architecture*, 2016.
- [44] Z. Jia, M. Maggioni, B. Staiger, and D. P. Scarpazza, “Dissecting the NVIDIA volta GPU architecture via microbenchmarking,” *CoRR*, 2018. [Online]. Available: <http://arxiv.org/abs/1804.06826>
- [45] Y. Jia, E. Shelhamer, J. Donahue, S. Karayev, J. Long, R. Girshick, S. Guadarrama, and T. Darrell, “Caffe: Convolutional architecture for fast feature embedding,” in *Proceedings of the 22nd ACM International Conference on Multimedia*, ser. MM ’14, 2014.
- [46] G. Pekhimenko, E. Bolotin, N. Vijaykumar, O. Mutlu, T. C. Mowry, and S. W. Keckler, “A case for toggle-aware compression for gpu systems,” *2016 IEEE International Symposium on High Performance Computer Architecture (HPCA)*, 2016.

- [47] G. Juckeland, W. C. Brantley, S. Chandrasekaran, B. M. Chapman, S. Che, M. E. Colgrove, H. Feng, A. Grund, R. Henschel, W. mei W. Hwu, H. Li, M. S. MÄijler, W. E. Nagel, M. Perminov, P. Shelepugin, K. Skadron, J. A. Stratton, A. Titov, K. Wang, G. M. van Waveren, B. Whitney, S. Wienke, R. Xu, and K. Kumaran, "Spec accel: A standard application suite for measuring hardware accelerator performance." 2014.
- [48] E. Choukse, M. Erez, and A. R. Alameldeen, "Compresspoints: An evaluation methodology for compressed memory systems," *IEEE Computer Architecture Letters*, vol. 17, 2018.
- [49] A. Krizhevsky, I. Sutskever, and G. E. Hinton, "Imagenet classification with deep convolutional neural networks," in *Proceedings of the 25th International Conference on Neural Information Processing Systems - Volume 1*, ser. NIPS'12, 2012.
- [50] C. Szegedy, V. Vanhoucke, S. Ioffe, J. Shlens, and Z. Wojna, "Rethinking the inception architecture for computer vision," *2016 IEEE Conference on Computer Vision and Pattern Recognition (CVPR)*, 2016.
- [51] F. N. Iandola, M. W. Moskewicz, K. Ashraf, S. Han, W. J. Dally, and K. Keutzer, "Squeezenet: Alexnet-level accuracy with 50x fewer parameters and <1mb model size," *CoRR*, vol. abs/1602.07360, 2016.
- [52] K. Simonyan and A. Zisserman, "Very deep convolutional networks for large-scale image recognition," *CoRR*, vol. abs/1409.1556, 2014.
- [53] K. He, X. Zhang, S. Ren, and J. Sun, "Deep residual learning for image recognition," *2016 IEEE Conference on Computer Vision and Pattern Recognition (CVPR)*, 2016.
- [54] J. Deng, W. Dong, R. Socher, L.-J. Li, K. Li, and L. Fei-Fei, "ImageNet: A Large-Scale Hierarchical Image Database," in *CVPR09*, 2009.
- [55] R. Józefowicz, O. Vinyals, M. Schuster, N. Shazeer, and Y. Wu, "Exploring the limits of language modeling," *CoRR*, vol. abs/1602.02410, 2016.
- [56] A. Bakhoda, G. Yuan, W. W. L. Fung, H. Wong, and T. M. Aamodt, "Analyzing CUDA Workloads Using a Detailed GPU Simulator," *IEEE International Symposium on Performance Analysis of Systems and Software (ISPASS)*, 2009.
- [57] A. Arunkumar, E. Bolotin, B. Cho, U. Milic, E. Ebrahimi, O. Villa, A. Jaleel, C.-J. Wu, and D. Nellans, "Mcm-gpu: Multi-chip-module gpus for continued performance scalability," in *Proceedings of the 44th Annual International Symposium on Computer Architecture*, ser. ISCA '17, 2017.
- [58] U. Milic, O. Villa, E. Bolotin, A. Arunkumar, E. Ebrahimi, A. Jaleel, A. Ramirez, and D. Nellans, "Beyond the socket: NUMA-aware GPUs," in *Proceedings of the 50th Annual IEEE/ACM International Symposium on Microarchitecture*. ACM, 2017, pp. 123–135.
- [59] V. Young, A. Jaleel, E. Bolotin, E. Ebrahimi, D. Nellans, and O. Villa, "Combining HW/SW Mechanisms to Improve NUMA Performance of Multi-GPU Systems," in *Proceedings of the 51th Annual IEEE/ACM International Symposium on Microarchitecture*. ACM, 2018.
- [60] NVIDIA. NVIDIA Pascal GPU Architecture. [Online]. Available: <https://www.nvidia.com/object/pascal-architecture-whitepaper.html>
- [61] ——. NVIDIA Volta GPU Architecture. [Online]. Available: <https://images.nvidia.com/content/volta-architecture/pdf/volta-architecture-whitepaper.pdf>
- [62] H. Qi, E. R. Sparks, and A. S. Talwalkar, "Paleo: a performance model for deep neural networks," 2017.
- [63] S. Lym, D. Lee, M. O'Connor, N. Chatterjee, and M. Erez, "DeLTA: GPU Performance Model for Deep Learning Applications with In-depth Memory System Traffic Analysis," in *Proceedings of the IEEE International Symposium on Performance Analysis of Systems and Software (ISPASS)*, 2019.
- [64] A. Krizhevsky, V. Nair, and G. Hinton, "Cifar-100 (canadian institute for advanced research)." [Online]. Available: <http://www.cs.toronto.edu/~kriz/cifar.html>
- [65] P. Goyal, P. Dollár, R. B. Girshick, P. Noordhuis, L. Wesolowski, A. Kyrola, A. Tulloch, Y. Jia, and K. He, "Accurate, large minibatch sgd: Training imagenet in 1 hour," *CoRR*, 2017.
- [66] C. J. Shallue, J. Lee, J. Antognini, J. Sohl-Dickstein, R. Frostig, and G. E. Dahl, "Measuring the effects of data parallelism on neural network training," *arXiv preprint arXiv:1811.03600*, 2018.
- [67] Y. Wu and K. He, "Group Normalization," in *ECCV*, 2018.
- [68] T.-Y. Lin, M. Maire, S. J. Belongie, L. D. Bourdev, R. B. Girshick, J. Hays, P. Perona, D. Ramanan, P. Dollár, and C. L. Zitnick, "Microsoft COCO: Common Objects in Context," in *ECCV*, 2014.